



## OPEN

## SUBJECT AREAS:

NANOSCIENCE AND  
TECHNOLOGY

ENGINEERING

NANOSCALE MATERIALS

NANOSCALE DEVICES

# Immersion Condensation on Oil-Infused Heterogeneous Surfaces for Enhanced Heat Transfer

Rong Xiao<sup>1</sup>, Nenad Miljkovic<sup>1</sup>, Ryan Enright<sup>1,2\*</sup> & Evelyn N. Wang<sup>1</sup><sup>1</sup>Department of Mechanical Engineering, Massachusetts Institute of Technology, Cambridge, Massachusetts, USA, <sup>2</sup>Stokes Institute, University of Limerick, Limerick, Ireland.Received  
13 March 2013Accepted  
30 May 2013Published  
13 June 2013Correspondence and  
requests for materials  
should be addressed to  
E.N.W. (enwang@mit.  
edu)\* Current address:  
Thermal Management  
Research Group,  
Efficient Energy  
Transfer ( $\eta$ ET) Dept.,  
Bell Labs Ireland,  
Alcatel-Lucent Ireland  
Ltd., Blanchardstown  
Business & Technology  
Park, Snugborough Rd,  
Dublin 15, Ireland.

Enhancing condensation heat transfer is important for broad applications from power generation to water harvesting systems. Significant efforts have focused on easy removal of the condensate, yet the other desired properties of low contact angles and high nucleation densities for high heat transfer performance have been typically neglected. In this work, we demonstrate immersion condensation on oil-infused micro and nanostructured surfaces with *heterogeneous* coatings, where water droplets nucleate immersed within the oil. The combination of surface energy heterogeneity, reduced oil-water interfacial energy, and surface structuring enabled drastically increased nucleation densities while maintaining easy condensate removal and low contact angles. Accordingly, on oil-infused heterogeneous nanostructured copper oxide surfaces, we demonstrated approximately 100% increase in heat transfer coefficient compared to state-of-the-art dropwise condensation surfaces in the presence of non-condensable gases. This work offers a distinct approach utilizing surface chemistry and structuring together with liquid-infusion for enhanced condensation heat transfer.

Condensation is an essential process in a wide variety of industrial applications including building environment<sup>1</sup>, power generation<sup>2</sup>, and water harvesting systems<sup>3</sup>. Enhancing condensation heat transfer has the potential to significantly improve efficiency and reduce the cost of these applications. In practice, filmwise condensation, where a thin liquid film covers the surface, is the most prevalent condensation mode due to the high wettability of common heat transfer materials. In this condensation mode, the heat transfer coefficient is limited by the thermal resistance associated with the condensate film which insulates the surface<sup>4</sup>. Accordingly, efforts spanning eight decades have been devoted to the realization of non-wetting surfaces for dropwise condensation where shedding droplets clear the surface for droplet re-nucleation/re-growth, leading to enhanced heat transfer rates<sup>5–10</sup>. One order of magnitude higher heat transfer coefficients compared to filmwise condensation have been reported using dropwise condensation in pure vapor environments<sup>6,7,10,11</sup>. In order to maximize the heat transfer coefficient, a high performance dropwise condensation surface should simultaneously achieve three properties: low contact angle hysteresis to minimize droplet departure radii, low contact angle to reduce the conduction resistance of the droplet, and high nucleation density<sup>12</sup>, as shown in Fig. 1 (see Supporting Information for detailed model derivation). Recently, investigations have focused on understanding how chemically modified micro/nanostructured surfaces can achieve superhydrophobicity to allow droplets to form in a stable Cassie wetting state<sup>13</sup>, which further improves droplet mobility and reduces the departure radii (Fig. 1a)<sup>9,14,15</sup>. In certain cases, these surfaces enable surface-tension-driven droplet jumping at micron length scales<sup>8,12,16</sup>. However, this focus on increasing the apparent hydrophobicity to reduce droplet departure radii does not necessarily address the other two aspects influencing condensation heat transfer rates. The high apparent contact angles of condensing droplets on superhydrophobic surfaces lead to an increase in the conduction resistance through the droplet<sup>12,17</sup>, hindering the overall heat transfer performance (Fig. 1b). Moreover, the Cassie wetting state introduces a vapor layer beneath the condensate droplet, which significantly increases the thermal resistance<sup>12</sup>. In addition, hydrophobic surface chemistry increases the nucleation thermodynamic energy barrier, thus reducing the nucleation density and limiting the heat transfer coefficient (Fig. 1c)<sup>18</sup>. Hydrophobic structured surfaces with well-defined hydrophilic sites on the roughness features have also been explored to control the nucleation density<sup>19</sup>, but strong droplet adhesion on such surfaces is likely to limit their applicability for condensation heat transfer enhancement. More recently, composite surfaces have been proposed whereby hydrophobic structured surfaces were infused with oil to simultaneously achieve easy droplet removal and low contact angles<sup>20–22</sup>. During

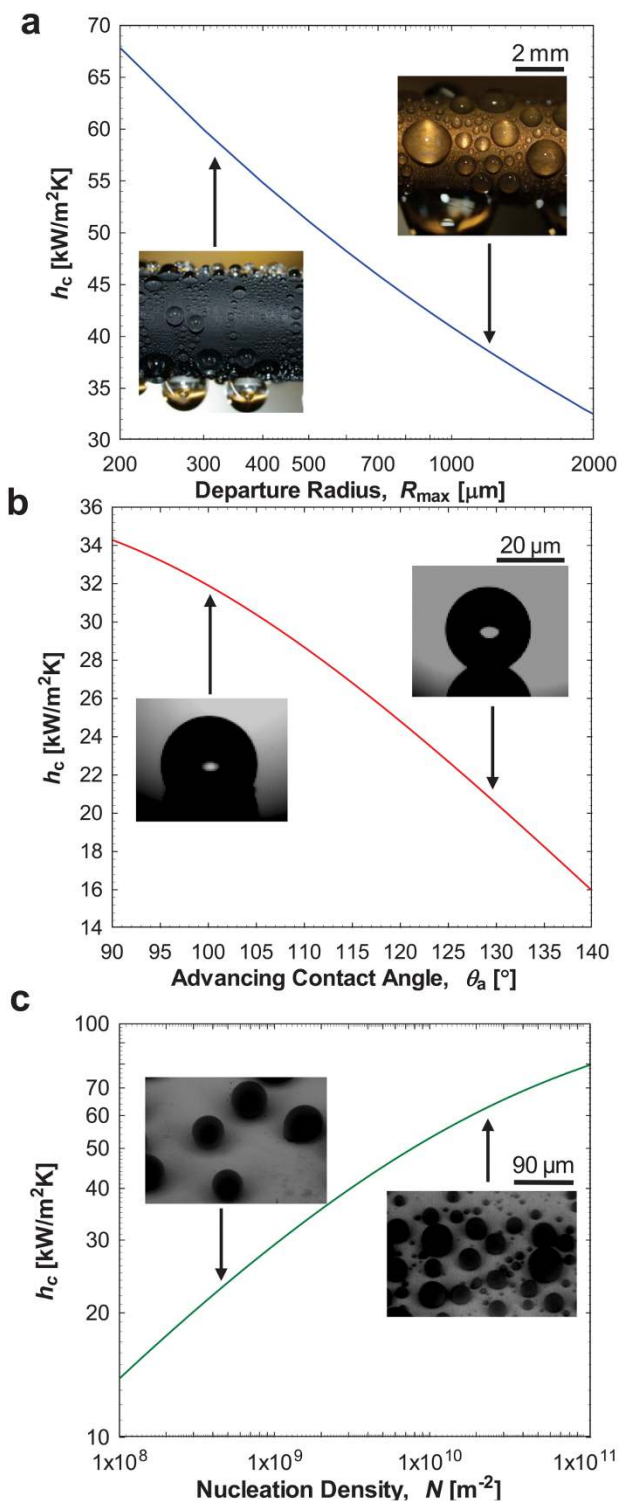


**Figure 1** | Parameters affecting condensation heat transfer coefficient. Model results showing influence of: (a) departure radius with advancing contact angle  $\theta_a = 110^\circ$  and nucleation density  $N = 10^{10} \text{ m}^{-2}$ , (b) advancing contact angle with nucleation density  $N = 10^{10} \text{ m}^{-2}$  and departure radius  $R_{\text{max}} = 800 \mu\text{m}$ , and (c) nucleation density with  $\theta_a = 110^\circ$  and  $R_{\text{max}} = 800 \mu\text{m}$ . The results assume a vapor pressure of 2700 Pa and surface temperature of  $20^\circ\text{C}$ .

condensation, two-tier surface roughness was shown to enhance the removal of droplets suspended *on top* of the infused oil layer<sup>21</sup>. While these works showed significant potential for enhanced condensation surfaces, achieving high nucleation densities has not previously been

considered. Furthermore, experimentally obtained heat transfer enhancements with such surfaces have not been reported.

In this work, we demonstrate immersion condensation, a new approach to enhance condensation heat transfer by introducing *heterogeneous* surface chemistry composed of discrete hydrophilic domains on a hydrophobic background in oil-infused micro and nanostructured surfaces. This approach allows water droplets to nucleate *immersed* within the oil to achieve high nucleation densities while maintaining easy droplet removal and low contact angles (Fig. 2a & b). In contrast to the same surface not infused with oil, nucleation densities were one order of magnitude larger due to the combined effect of the high-surface-energy sites and the reduced oil-water interfacial energy which, together, lower the thermodynamic energy barrier for stable nuclei formation. Meanwhile, the contact angle hysteresis was as low as  $3^\circ$  and the droplet apparent contact angle was  $\approx 110^\circ$ . We demonstrate that the immersion of droplets in the presence of the heterogeneous coating is essential to the high water nucleation densities and significant heat transfer enhancements. We first characterized the heterogeneous coating on flat silicon surfaces using an Atomic Force Microscope (AFM). The scans showed the presence of discrete high-surface-energy sites on a low-surface-energy background. Well-defined micropillar arrays were subsequently coated and then infused with oil to study the physics of condensation behavior. Finally, with our increased understanding of the phenomenon, we experimentally demonstrated heat transfer enhancements of approximately 100% with oil-infused, heterogeneously coated copper oxide nanostructured surfaces in comparison with state-of-the-art dropwise condensing surfaces, which suggests the practicality of our approach. This work promises the development of a scalable strategy for highly efficient condensation heat transfer for industrial, building energy, electronics cooling, and water-harvesting applications.

## Results

**Surface heterogeneity by self-assembled coatings.** We deposited a self-assembled coating (SAC) of (tridecafluoro-1,1,2,2-tetrahydrooctyl)-1-trichlorosilane (TFTS) from the vapor phase (See Methods for the deposition process). The SAC coating method is capable of forming heterogeneity by agglomeration<sup>23</sup>. We chose the SAC method due to its simplicity and scalability, but alternative methods are also available to generate heterogeneity at the appropriate length scale, *e.g.*, block copolymer or nano-imprinting<sup>24,25</sup>. Height and phase AFM images of the TFTS coating on a smooth silicon surface were obtained and are shown in Fig. 2c & d, respectively, where the white spots are the nanoscale agglomerates of TFTS ( $\approx 200\text{--}500 \text{ nm}$  in diameter). The phase angle of the agglomerates was significantly higher than that of the background, indicating that the agglomerates have higher surface energy<sup>26</sup>. We determined the local contact angle of water on the high-surface-energy agglomerates to be  $60^\circ \pm 1.5^\circ$  by measuring the advancing and receding contact angle of a water droplet on the smooth, coated surface in air ( $\theta_a/\theta_r = 122^\circ \pm 1.3^\circ/78^\circ \pm 1.3^\circ$ ) and interpreting the data using a modified Cassie-Baxter model that incorporates the effect of local contact line deformation<sup>27</sup>.

**Immersion condensation on silicon micropillars.** Next, we deposited the SAC on silicon micropillar arrays to fundamentally investigate nucleation behavior on oil-infused surfaces. We fabricated silicon micropillar arrays with diameters,  $d$ , ranging from 0.4–5  $\mu\text{m}$ , periods,  $l$ , ranging from 4–25  $\mu\text{m}$ , and heights,  $h$ , ranging from 10–25  $\mu\text{m}$  using contact lithography and deep reactive ion etching (DRIE) processes. The geometries were chosen to satisfy the imbibition condition to enable oil spreading<sup>28</sup> and to stabilize the oil film<sup>20</sup>. The pillar surfaces were subsequently functionalized with the TFTS SAC, and infused with a fluorinated oil, Krytox GPL 100. The low surface tension of Krytox oil ( $\approx 17\text{--}19 \text{ mN/m}$ ) allowed

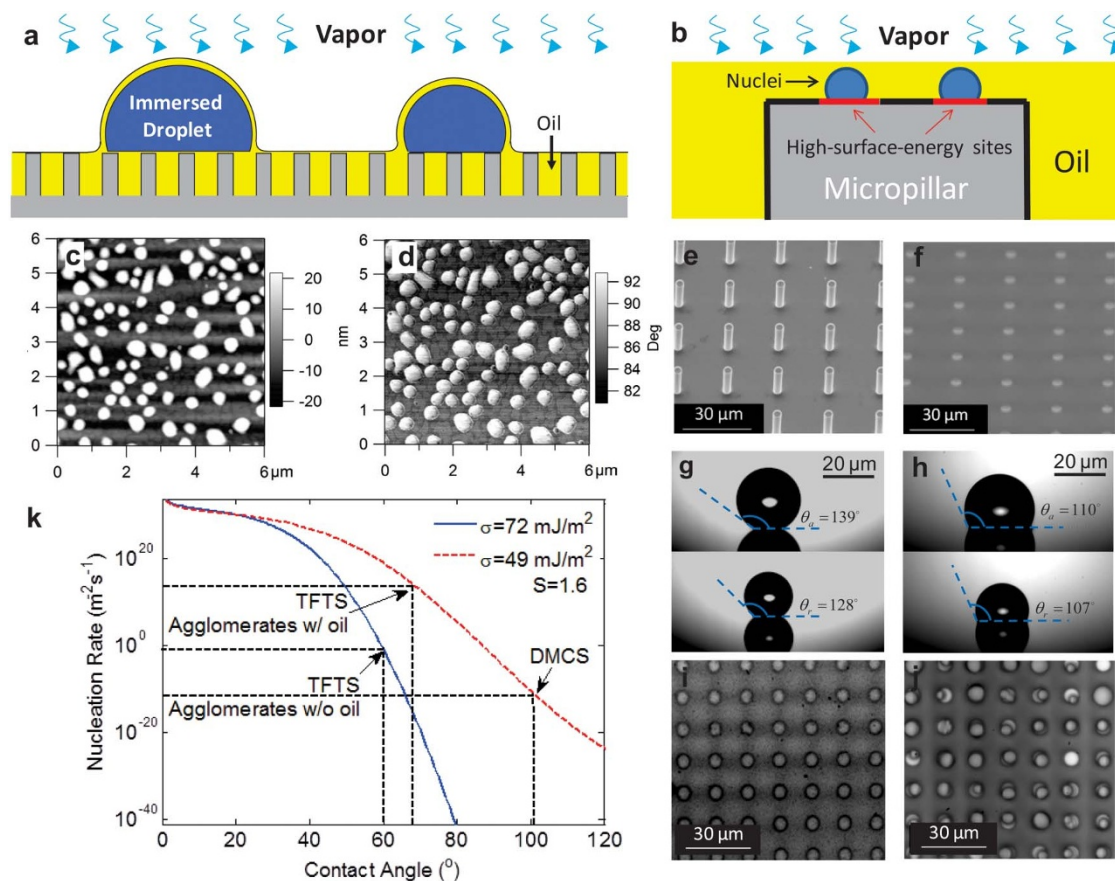


**Figure 2 | Mechanism of immersion condensation.** (a) Schematic showing water vapor diffusing through the thin oil film and forming immersed droplets on the tips of micropillars. (b) Magnified schematic showing the nuclei formation on high-surface-energy sites on micropillar tips in the oil. (c) and (d) Height and phase images of atomic force microscope (AFM) images of TFTS ((Tridecafluoro-1,1,2,2-tetrahydrooctyl)-1-trichlorosilane) coating. The higher phase angle at the nanoagglomerates indicates local higher surface energy. (e) and (f) Environmental scanning electron microscope (ESEM) images of TFTS-coated micropillar arrays before and after the oil-infusion. (g) and (h) Contact angle hysteresis on a superhydrophobic surface without and with oil-infusion. The hysteresis is  $\approx 3^\circ$  on the oil-infused surface with a contact angle  $\approx 110^\circ$ . The microstructure geometries were the same on both surfaces, with diameter of  $5\ \mu\text{m}$ , height of  $20\ \mu\text{m}$ , and period of  $15\ \mu\text{m}$ . (i) and (j) White-light optical microscope images of condensation on micropillar arrays before and after oil-infusion. The micropillar geometries were the same as (g) and (h). The supersaturation in the experiments was  $S = 1.6$ . (k) Nucleation rates predicted as a function of contact angle and interfacial energy.

it to spread on the surface and form a stable film *via* capillarity. A dry  $\text{N}_2$  stream was used to assist spreading and remove excess oil. Typical environmental scanning electron microscope (ESEM) images of the coated pillar arrays without and with oil-infusion are shown in Fig. 2e & f, respectively. On these TFTS-coated pillar arrays, the advancing and receding contact angles without oil-infusion were  $\theta_a/\theta_r = 139^\circ \pm 3^\circ/128^\circ \pm 3^\circ$ , whereas those with oil-infusion were  $\theta_a/\theta_r = 110^\circ \pm 2^\circ/107^\circ \pm 2^\circ$  (Fig. 2g & h). Such low contact angle hysteresis is a key attribute for allowing droplets to be removed with a small departure radius under gravity during condensation<sup>20,21,29</sup>. Figures 2i & j show white light optical microscope images comparing the drastic difference in nucleation density during condensation without and with oil-infusion on the TFTS-coated micropillar arrays, respectively (see Methods for the experimental procedure). Under the prescribed supersaturation of  $S = 1.6$  ( $S = p_v/p_w$  where  $p_v$  is the water vapor pressure and  $p_w$  is the water saturation pressure associated with the surface temperature), nucleation was rarely observed on the surface without oil-infusion (nucleation density  $N \approx (4 \pm 2) \times 10^8\ \text{m}^{-2}$ ) (Fig. 2i), but was observed on every tip of the pillars after oil-infusion (nucleation density  $N \approx (4.4 \pm 0.2) \times 10^9\ \text{m}^{-2}$ ) (Fig. 2j). Nucleation in the space between the pillars was not observed due to the large thickness of oil coverage that limits water vapor diffusion to the SAC. Meanwhile, nucleation on the oil/vapor interface did not occur due to the low interfacial energy.

The increase in nucleation density on the oil-infused TFTS surfaces was achieved *via* the combination of the high-surface-energy sites and reduced water-oil interfacial energy. Based on classical nucleation theory, the nucleation rate can be determined as a function of the contact angle and the surface energy of the condensate at a given supersaturation, as shown in Fig. 2k (see Supporting Information for the detailed derivation)<sup>18,30–32</sup>. On the oil-infused surface, the tips of the pillars were covered by oil due to its low surface tension. However, the tips were still visible in the ESEM images (Fig. 2f) because of the small thickness of the oil film. In these regions, the water vapor is able to diffuse through the thin oil layer and form nuclei immersed in the oil layer on the high-surface-energy sites. The critical sizes of nuclei ( $< 10\ \text{nm}$ ) were much smaller than the sizes of the high-surface-energy sites ( $\approx 200\text{--}500\ \text{nm}$ ) so that the local contact angles of the nuclei are only determined by the high-surface-energy sites. With the introduction of oil, the local contact angle of nuclei on those high-surface-energy domains can be bounded in the range from  $43^\circ$  to  $67^\circ$  using Young's equation (see Supporting Information). As a result, the energy threshold for nucleation was significantly decreased due to the low local contact angle, in combination with the reduced interfacial energy between water and oil ( $\approx 49\ \text{mJ/m}^2$ )<sup>21</sup> compared to that between water and vapor ( $\approx 72\ \text{mJ/m}^2$ ). Accordingly, as shown in Fig. 2k, assuming a local contact angle lower than  $67^\circ$ , the predicted nucleation rate increases



from  $0.2 \text{ m}^{-2}\text{s}^{-1}$  to greater than  $10^{14} \text{ m}^{-2}\text{s}^{-1}$  due to the encapsulating oil phase in comparison with the same surface without oil-infusion. The oil encapsulation is essential in reducing the energy barrier for nuclei formation and enhancing nucleation density, which is distinct from previous work where the encapsulating oil phase was considered as unfavorable for condensation<sup>21</sup>. The calculated nucleation rate allows the nucleation density to be orders of magnitude larger than the density of the high-surface energy domains. As a result, multiple nuclei could form on each tip of the pillars where the oil layer is thin enough for effective vapor diffusion. However, due to the resolution limits of our imaging experiments, only a single droplet was apparent on each pillar tip. Therefore, we only determined an order of magnitude increase in the *observed* nucleation density, which was equal to the density of the pillars (Fig. 2j). We also performed control condensation experiments on oil-infused micropillar arrays with dimethyldichlorosilane (DMCS), which is a *homogeneous* hydrophobic coating with advancing and receding contact angles of  $\theta_a/\theta_r = 103.8^\circ \pm 0.5^\circ/102.7^\circ \pm 0.4^\circ$  (see Supporting Information for details of the control experiments). We found no observable change in nucleation density after oil-infusion on the DMCS coated surfaces, as predicted by theory (Fig. 2k). These results further support the idea that a high performance condensation surface can be achieved through the combination of local high-surface-energy sites and oil-infusion, which has not been demonstrated previously. However, the overall surface needs to be hydrophobic to prevent the spreading of the condensate beneath the oil film and maintain easy droplet removal. Otherwise, the condensate would wet the substrate, disrupting the oil film and resulting in droplet pinning.

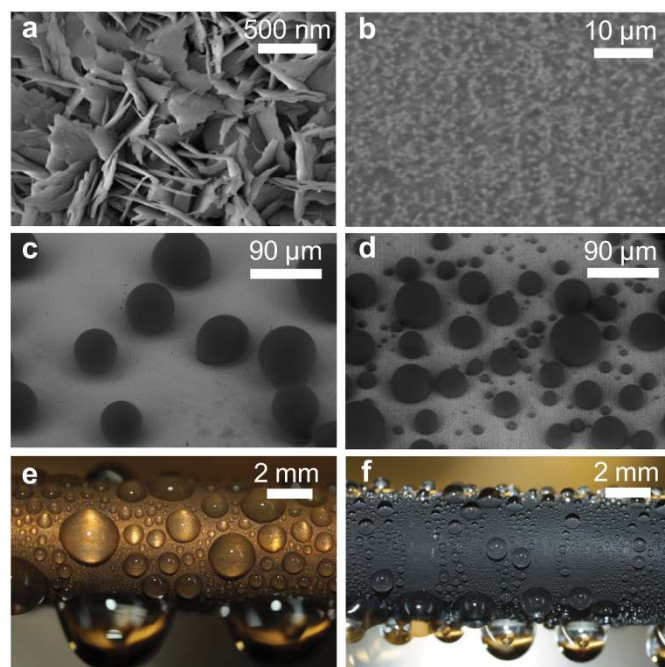


**Figure 3 | Scalable copper oxide (CuO) surfaces for immersion condensation.** (a) Field emission SEM (FESEM) image of CuO nanostructures. (b) Environmental SEM (ESEM) image of CuO nanostructures infused with Krytox oil. (c) ESEM image of nucleation on TFTS-coated CuO surface. (d) ESEM image of oil-infused TFTS-coated CuO surface. An order of magnitude higher nucleation density was observed compared to (c). (e) Image of dropwise condensation on a hydrophobic copper tube surface. (f) Image of condensation on an oil-infused TFTS-coated CuO surface. Significantly higher droplet density was observed on the oil-infused surface while a low departure radius of  $0.98 \pm 0.13 \text{ mm}$  was maintained.

**Immersion condensation on scalable copper oxide nanostructures.** Next, we studied the overall heat transfer performance of an immersion condensation surface. While studies on well-defined silicon micropillar arrays can provide physical insight into immersion condensation behavior, they are not practical due to cost and challenges in interfacing the silicon substrate and our heat transfer measurement apparatus with minimum uncertainties. Therefore, we performed immersion condensation heat transfer measurements on oil-infused copper oxide (CuO) nanostructures functionalized with TFTS, which promises a scalable, low cost platform for condensation surfaces<sup>33</sup>. ESEM images of representative copper oxide nanostructures without and with Krytox oil-infusion are shown in Fig. 3a & b, respectively. Condensation experiments were performed on the CuO surfaces without and with oil-infusion in an environmental SEM with  $1 < S < 1.29$  for visualization (see Methods for detailed imaging process)<sup>12</sup>. The Figures 3c & d show an order of magnitude increase in nucleation density on the oil-infused surface, as similarly observed on the silicon-based microstructures. To capture the condensation heat transfer behavior, we formed the oil-infused heterogeneous CuO surfaces on copper tubes (see Methods for detailed fabrication process). Figures 3e & f show condensation on a typical dropwise hydrophobic surface and an oil-infused heterogeneous immersion condensation surface, respectively. Significantly higher droplet densities were observed on the oil-infused surface. Meanwhile, the average shedding radius of droplets was reduced from  $\hat{R}_{DHP} = 1.83 \pm 0.31 \text{ mm}$  on the typical dropwise hydrophobic surfaces to  $\hat{R}_{IC} = 0.98 \pm 0.13 \text{ mm}$  on the immersion condensation surfaces (see Supporting Information for details on determining the droplet shedding radii). Prior to droplet departure, the droplets grew orders of magnitude larger than the characteristic length scale of the nanostructures, thus high apparent contact angles of the droplet ( $\approx 110^\circ$ ) were observed, consistent with the low surface energy of the solid-oil composite surface.

Overall heat transfer coefficients were measured to evaluate the performance on three different Cu-based surfaces: a hydrophobic surface for typical dropwise condensation, a superhydrophobic TFTS-coated CuO surface, and a Krytox oil-infused, TFTS-coated CuO surface (Fig. 4) (see Methods and Supporting Information for detailed experimental process). The Krytox GPL 100 oil evaporates completely when the test chamber is evacuated to pressures lower

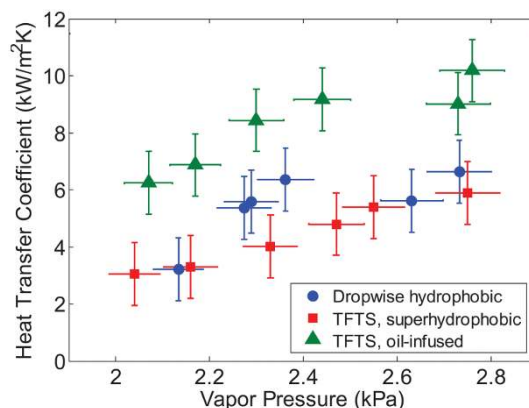


**Figure 4 | Experimental immersion condensation heat transfer measurement.** Comparison of overall heat transfer coefficient during condensation on the hydrophobic surface, TFTS-coated superhydrophobic surface, and oil-infused composite surface with an initial chamber pressure of 30 Pa (primarily non-condensable gases). The supersaturation was varied in the range  $1 < S < 1.6$ . The heat transfer coefficient on the oil-infused surface increased by approximately 100% compared to the dropwise and superhydrophobic surfaces.



than 1 Pa. Therefore, we set the initial chamber pressure as high as 30 Pa (primarily composed of non-condensable gases, NCG) to avoid the evaporation of oil with steam pressures ranging from 2 to 3 kPa ( $1 < S < 1.6$ ) in the experiments. This is consistent with actual condenser systems where NCG partial pressures are typically found in the range of 30 Pa and significantly affect the condensation heat transfer performance<sup>34–37</sup>. Accordingly, with these experimental conditions, we were able to emulate a more realistic condensation environment and demonstrate the practical significance of the immersion condensation mode. While the superhydrophobic surface is more hydrophobic than the typical dropwise hydrophobic surface, flooding and strong pinning of the condensate was observed due to the high supersaturation conditions ( $S$  as high as 1.6), leading to similar heat transfer coefficients with the typical dropwise hydrophobic surfaces. Note that these results are distinct from previous literature where jumping of droplets on superhydrophobic surfaces increased heat transfer coefficients at lower saturation conditions ( $S < 1.12$ )<sup>16,38</sup>. In addition, the overall heat transfer coefficients on DHP surfaces in this work ( $h \approx 2\text{--}7 \text{ kW/m}^2\text{K}$ ) are much lower compared to pure vapor conditions ( $h \approx 12\text{--}13 \text{ kW/m}^2\text{K}$ )<sup>16</sup> due to the presence of NCGs acting as a diffusion barrier to the transport of water vapor towards the condensing surface. In comparison to the typical hydrophobic surfaces, the Krytox oil-infused TFTS-coated CuO surface demonstrated approximately a 100% improvement in heat transfer coefficient over the entire range of supersaturations tested ( $1 < S < 1.6$ ) with the existence of NCGs. While the available condensation area was reduced due to the oil coverage, the significant improvement in the overall heat transfer coefficient highlights the collective role of enhanced nucleation density, more frequent droplet removal, and lower droplet contact angle (Fig. 1).

## Discussions

Oil-impregnated surfaces have been recently reported as a promising approach to enhance condensation heat transfer surfaces due to the ultra-low droplet adhesion<sup>20–22</sup>. However, easy droplet removal is not the only desired property for high heat transfer performance. Low contact angle and high nucleation densities are also essential to further enhance condensation heat transfer. In this work, we have demonstrated that by combining surface heterogeneity and oil-infusion, the nucleation density in condensation can be increased by over an order of magnitude *via* immersion condensation while maintaining low droplet adhesion, which has not been observed previously. The increase in nucleation densities *via* the combined effect of heterogeneity and the reduced oil-water interfacial tension was explained by our model based on classical nucleation theory, and was also corroborated with control experiments using silane-coated silicon micropillar arrays. With improved understanding of the physics, we investigated oil-infused superhydrophobic copper oxide surfaces as a platform for condensation enhancement in practical systems. We demonstrated that the condensation heat transfer coefficient on such oil-infused heterogeneous surfaces can be enhanced by approximately 100% compared to state-of-the-art dropwise surfaces in the presence of non-condensables gases. Based on previous condensation heat transfer models shown in Fig. 1, an order of magnitude increase in nucleation density could contribute to approximately 80% increase in the overall heat transfer coefficient. Meanwhile, the low departure radii and low contact angle also assisted in the total improvement. Achieving the three key aspects of condensation simultaneously is essential to realize heat transfer enhancement by as high as 100%. Further work is needed to tailor oil and coating properties, as well as surface geometry to minimize oil loss during operation and maximize condensing surface area. With continued development, immersion condensation promises to be an important condensation mode for a variety of heat transfer and resource conserving applications.

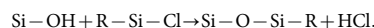
## Methods

**Surface fabrication.** The silicon micropillar arrays were fabricated using contact lithography followed by deep reactive ion etching. For copper oxide surfaces, we used commercially available oxygen-free Cu tubes (99.9% purity) with outer diameters,  $D_{OD} = 6.35 \text{ mm}$ , inner diameters,  $D_{ID} = 3.56 \text{ mm}$ , and lengths  $L = 131 \text{ mm}$  as the test samples for the experiments. Each Cu tube was cleaned in an ultrasonic bath with acetone for 10 minutes and rinsed with ethanol, isopropyl alcohol and de-ionized (DI) water. The tubes were then dipped into a 2.0 M hydrochloric acid solution for 10 minutes to remove the native oxide film on the surface, then triple-rinsed with DI water, and dried with clean nitrogen gas.

Nanostructured CuO films were formed by immersing the cleaned tubes into a hot ( $96 \pm 3^\circ\text{C}$ ) alkaline solution composed of  $\text{NaClO}_2$ ,  $\text{NaOH}$ ,  $\text{Na}_3\text{PO}_4 \cdot 12\text{H}_2\text{O}$ , and DI water (3.75 : 5 : 10 : 100 wt.%)<sup>33,39</sup>. During the oxidation process, a thin ( $< 200 \text{ nm}$ )  $\text{Cu}_2\text{O}$  layer was formed that then re-oxidized to form sharp, knife-like CuO structures with heights of  $h \approx 1 \mu\text{m}$ , solid fraction<sup>39</sup>  $\phi \approx 0.023$  and roughness factor<sup>39</sup>  $r \approx 10$ . To verify the independence of oxide thickness on chemical oxidation time<sup>40</sup>, four separate samples were made using oxidation times,  $\tau = 5, 10, 20, \text{ and } 45 \text{ minutes}$ . The sharp CuO structures were then coated with a silane SAC to create SHP surfaces.

In addition to SHP surfaces, cleaned copper tubes were also immersed into hydrogen peroxide solutions at room temperature to form a thin smooth layer of  $\text{Cu}_2\text{O}$ . The smooth surfaces were also coated with TFTS to achieve typical hydrophobic surfaces for dropwise condensation (DHP).

**Surface coating deposition.** The self-assembled coatings (SAC) were formed using a vapor deposition process. First, the silicon surfaces were cleaned using a Piranha solution ( $\text{H}_2\text{O}_2\text{:H}_2\text{SO}_4 = 1 : 3$ ) to remove possible organic contamination and to create a large number of  $-\text{OH}$  bonds on the surface, which enables the bonding between silane molecules and the silicon surface. For the copper oxide surfaces, the surfaces were cleaned by intensive plasma ( $\approx 1 \text{ hr}$ ). The samples were then placed in a desiccator (Cole-Palmer) together with a small petri dish containing  $\approx 1 \text{ mL}$  of the silane liquid. The desiccator was pumped down to  $\approx 10 \text{ kPa}$ . The pump was then shut off and the valve was closed so that the silane liquid could evaporate in the low-pressure environment of the desiccator and attach to the surfaces to form the SAC *via* the following reaction,



During the self-assembly process, the silane molecules form nanoscale agglomerates with diameters of  $\approx 200\text{--}500 \text{ nm}$  shown in Figure 2c and d, as reported previously<sup>23</sup>. After 30 minutes of reaction, the desiccator was vented and the samples were rinsed using de-ionized (DI) water. Such vapor deposition process was used for both TFTS and Dimethyldichlorosilane (DMCS) coatings, but in dedicated desiccators to avoid cross-contamination of the different silane molecules.

**Surface characterization.** Advancing and receding contact angles for all samples were measured and analyzed using a micro-goniometer (MCA-3, Kyowa Interface Science Co., Japan). Field emission electron microscopy was performed on a Zeiss Ultra Plus FESEM (Carl Zeiss GMBH) at an imaging voltage of 3 kV.

**OM imaging procedure.** The samples were horizontally mounted on a thermal stage inside an enclosure and cooled to  $T_w = 283.1 \pm 0.1 \text{ K}$  in a dry nitrogen atmosphere. Following thermal equilibration ( $\approx 5 \text{ minutes}$ ), nucleation was initiated by flowing water-saturated nitrogen into the enclosure. The humidity of the gas flow was measured using a humidity probe located 1 cm above the sample to determine the supersaturation,  $S$ , defined as the ratio of the vapor pressure to the saturation pressure at the stage temperature ( $S = p_v/p_{s,w}$ ). Typical values of supersaturation were  $S \approx 1.6$ . The nucleation density and subsequent growth behavior was recorded at a frame rate of 10 frames per second using a high speed camera (Phantom V7.1, Vision Research) attached to the optical microscope. The observable nucleation density during each experiment was determined by counting the number of nuclei in the captured images and dividing the number of nuclei by the imaging area. Multiple experiments were performed to determine the average nucleation densities on the different surfaces.

**ESEM imaging procedure.** Condensation nucleation and growth were studied on these fabricated surfaces using an environmental scanning electron microscope (EVO 55 ESEM, Carl Zeiss GMBH). Backscatter detection mode was used with a high gain. The water vapor pressure in the ESEM chamber was  $800 \pm 80 \text{ Pa}$ . Typical image capture was obtained with a beam potential of 20 kV and variable probe current depending on the stage inclination angle. To limit droplet heating effects, probe currents were maintained below 2.0 nA and the view area was kept above  $400 \mu\text{m} \times 300 \mu\text{m}^2$ . A  $500 \mu\text{m}$  lower aperture was used in series with a  $100 \mu\text{m}$  variable pressure upper aperture to obtain greater detail. The sample temperature was initially set to  $4 \pm 1.5^\circ\text{C}$  and was allowed to equilibrate for 5 minutes. The surface temperature was subsequently decreased to  $3 \pm 1.5^\circ\text{C}$ , resulting in nucleation of water droplets on the sample surface. Accordingly, the supersaturation,  $S$ , during the imaging process was in the range of  $1 < S < 1.29$ . Images and recordings were obtained at an inclination angle of  $45^\circ$  from the horizontal to observe droplet growth. Cu tape was used for mounting the sample to the cold stage to ensure good thermal contact.

**Heat transfer measurements.** The test samples, 6.35 mm diameter tubes with different surface treatments, were placed in an environmental chamber (Kurt J. Lesker) for the heat transfer measurements. A water reservoir, which was connected to the chamber *via* a vapor valve, was heated to  $> 95^\circ\text{C}$  to produce steam. The vapor



valve was opened to allow steam to flow into the chamber after the chamber was pumped down to the targeted non-condensable pressure ( $\approx 30$  Pa). Chilled water flowed along the inside of the tube where the inlet temperature and outlet temperature were both measured by thermocouples so that the heat flux could be determined by the temperature rise. The temperature difference,  $\Delta T$  was determined as the log-mean temperature difference (LMTD) between the vapor and the chilled water. Each data point in Figure 4 of the manuscript was determined over 10 minutes of steady state operation. The vapor inflow valve was then adjusted to change the vapor pressure in the chamber. More details of the experiment procedure can be found in Supplementary Information Section S5.

- Pérez-Lombard, L., Ortiz, J. & Pout, C. A review on buildings energy consumption information. *Energy and Buildings* **40**, 394–398 (2008).
- Beér, J. M. High efficiency electric power generation: The environmental role. *Progress in Energy and Combustion Science* **33**, 107–134 (2007).
- Khawaji, A. D., Kutubkhanah, I. K. & Wie, J.-M. Advances in seawater desalination technologies. *Desalination* **221**, 47–69 (2008).
- Mills, A. F. *Heat and Mass Transfer*. 2 edn, (Prentice-Hall, 1999).
- Schmidt, E., Schurig, W. & Sellschopp, W. Versuche über die Kondensation von Wasserdampf in Film- und Tropfenform. *Forschung im Ingenieurwesen* **1**, 53–63 (1930).
- Tanner, D. W., Potter, C. J., Pope, D. & West, D. Heat transfer in dropwise condensation—Part I The effects of heat flux, steam velocity and non-condensable gas concentration. *International Journal of Heat and Mass Transfer* **8**, 419–426 (1965).
- O'Neill, G. A. & Westwater, J. W. Dropwise condensation of steam on electroplated silver surfaces. *International Journal of Heat and Mass Transfer* **27**, 1539–1549 (1984).
- Boreyko, J. B. & Chen, C.-H. Self-Propelled Dropwise Condensate on Superhydrophobic Surfaces. *Phys Rev Lett* **103**, 184501 (2009).
- Chen, C.-H. *et al.* Dropwise condensation on superhydrophobic surfaces with two-tier roughness. *Appl Phys Lett* **90**, 173108–173103 (2007).
- Le Fevre, E. J. & Rose, J. W. An experimental study of heat transfer by dropwise condensation. *International Journal of Heat and Mass Transfer* **8**, 1117–1133 (1965).
- Daniel, S., Chaudhury, M. K. & Chen, J. C. Fast Drop Movements Resulting from the Phase Change on a Gradient Surface. *Science* **291**, 633–636 (2001).
- Miljkovic, N., Enright, R. & Wang, E. N. Effect of Droplet Morphology on Growth Dynamics and Heat Transfer during Condensation on Superhydrophobic Nanostructured Surfaces. *ACS Nano* **6**, 1776–1785 (2012).
- Cassie, A. B. D. & Baxter, S. Wettability of porous surfaces. *T Faraday Soc* **40**, 0546–0550 (1944).
- Enright, R., Miljkovic, N., Al-Obeidi, A., Thompson, C. V. & Wang, E. N. Condensation on Superhydrophobic Surfaces: The Role of Local Energy Barriers and Structure Length Scale. *Langmuir* **28**, 14424–14432 (2012).
- Rykaczewski, K. *et al.* How nanorough is rough enough to make a surface superhydrophobic during water condensation? *Soft Matter* **8**, 8786–8794 (2012).
- Miljkovic, N. *et al.* Jumping-Droplet-Enhanced Condensation on Scalable Superhydrophobic Nanostructured Surfaces. *Nano Lett* **13**, 179–187 (2013).
- Kim, S. & Kim, K. J. Dropwise Condensation Modeling Suitable for Superhydrophobic Surfaces. *Journal of Heat Transfer* **133**, 081502 (2011).
- Kashchiev, D. *Nucleation: Basic Theory with Applications*. 1 edn, (Oxford: Butterworth-Heinemann, 2000).
- Varanasi, K. K., Hsu, M., Bhat, N., Yang, W. & Deng, T. Spatial control in the heterogeneous nucleation of water. *Appl Phys Lett* **95**, 094101–094103 (2009).
- Wong, T.-S. *et al.* Bioinspired self-repairing slippery surfaces with pressure-stable omniphobicity. *Nature* **477**, 443–447 (2011).
- Anand, S., Paxson, A. T., Dhiman, R., Smith, J. D. & Varanasi, K. K. Enhanced Condensation on Lubricant Impregnated Nanotextured Surfaces. *ACS Nano* **6**, 10122–10129 (2012).
- Mishchenko, L. *et al.* Design of Ice-free Nanostructured Surfaces Based on Repulsion of Impacting Water Droplets. *ACS Nano* **4**, 7699–7707 (2010).
- Bunker, B. C. *et al.* The Impact of Solution Agglomeration on the Deposition of Self-Assembled Monolayers. *Langmuir* **16**, 7742–7751 (2000).
- Park, M., Harrison, C., Chaikin, P. M., Register, R. A. & Adamson, D. H. Block Copolymer Lithography: Periodic Arrays of  $\sim 1011$  Holes in 1 Square Centimeter. *Science* **276**, 1401–1404 (1997).
- Guo, L. J., Cheng, X. & Chou, C.-F. Fabrication of Size-Controllable Nanofluidic Channels by Nanoimprinting and Its Application for DNA Stretching. *Nano Lett* **4**, 69–73 (2003).
- James, P. J. *et al.* Interpretation of Contrast in Tapping Mode AFM and Shear Force Microscopy. A Study of Nafion. *Langmuir* **17**, 349–360 (2000).
- Raj, R., Enright, R., Zhu, Y., Adera, S. & Wang, E. N. Unified Model for Contact Angle Hysteresis on Heterogeneous and Superhydrophobic Surfaces. *Langmuir* **28**, 15777–15788 (2012).
- Bico, J., Thiele, U. & Quéré, D. Wetting of textured surfaces. *Colloids and Surfaces A: Physicochemical and Engineering Aspects* **206**, 41–46 (2002).
- Dimitrakopoulos, P. & Higdon, J. J. L. On the gravitational displacement of three-dimensional fluid droplets from inclined solid surfaces. *Journal of Fluid Mechanics* **395**, 181–209 (1999).
- Blander, M. & Katz, J. L. Bubble Nucleation in Liquids. *Aiche Journal* **21**, 833–848 (1975).
- Hirth, J. P. & Pound, G. M. *Condensation and evaporation - nucleation and growth kinetics* (England: Pergamon Press., 1963).
- Pound, G. M., Simnad, M. T. & Yang, L. Heterogeneous Nucleation of Crystals from Vapor. *The Journal of Chemical Physics* **22**, 1215–1219 (1954).
- Miljkovic, N. & Wang, E. N. Condensation heat transfer on superhydrophobic surfaces. *MRS Bulletin* **38**, 397–406 (2013).
- Rose, J. W. Dropwise condensation theory and experiment: A review. *Proceedings of the Institution of Mechanical Engineers, Part A: Journal of Power and Energy* **216**, 115–128 (2002).
- Denny, V. E. & Jusonius, V. J. Effects of noncondensable gas and forced flow on laminar film condensation. *International Journal of Heat and Mass Transfer* **15**, 315–326 (1972).
- Sparrow, E. M., Minkowycz, W. J. & Saddy, M. Forced convection condensation in the presence of noncondensables and interfacial resistance. *International Journal of Heat and Mass Transfer* **10**, 1829–1845 (1967).
- Tanner, D. W., Pope, D., Potter, C. J. & West, D. Heat transfer in dropwise condensation at low steam pressures in the absence and presence of non-condensable gas. *International Journal of Heat and Mass Transfer* **11**, 181–190 (1968).
- Miljkovic, N., Enright, R. & Wang, E. N. Modeling and Optimization of Superhydrophobic Condensation. *Journal of Heat Transfer*, DOI: 10.1115/1.4024597.
- Enright, R., Miljkovic, N., Dou, N., Nam, Y. & Wang, E. N. Condensation on Superhydrophobic Copper Oxide Nanostructures. *Journal of Heat Transfer*, DOI: 10.1115/1.4024424.
- Nam, Y. & Sungtaek, Y. A comparative study of the morphology and wetting characteristics of micro/nanostructured Cu surfaces for phase change heat transfer applications. *Journal of Adhesion Science and Technology*, DOI:10.1080/01694243.2012.697783.
- Rykaczewski, K., Scott, J. H. J. & Fedorov, A. G. Electron beam heating effects during environmental scanning electron microscopy imaging of water condensation on superhydrophobic surfaces. *Appl Phys Lett* **98**, (2011).

## Acknowledgements

The authors gratefully acknowledge the funding support from the Office of Naval Research (ONR) with Dr. Mark Spector as the project manager, and the MIT S3TEC Center, an Energy Frontier Research Center funded by the Department of Energy, Office of Science, Office of Basic Energy Sciences. R. E. acknowledges funding received from the Irish Research Council for Science, Engineering, and Technology, co-funded by Marie Curie Actions under FP7. The authors would also like to thank the MIT Microsystems Technology Lab for fabrication staff support, help, and use of equipment. This work was performed in part at the Center for Nanoscale Systems (CNS), a member of the National Nanotechnology Infrastructure Network (NNIN), which is supported by the National Science Foundation under NSF award no. ECS-0335765. CNS is part of Harvard University.

## Author contributions

R.X., R.E., N.M. and E.N.W. conceived the initial idea of this research. E.N.W. guided the work. R.X. and N.M. carried out the experiments and collected data. R.X., R.E. and N.M. analyzed the data. N.M. carried out the theoretical analysis. R.X., N.M., R.E. and E.N.W. were responsible for writing the paper.

## Additional information

**Supplementary information** accompanies this paper at <http://www.nature.com/scientificreports>

**Competing financial interests:** The authors declare no competing financial interests.

**How to cite this article:** Xiao, R., Miljkovic, N., Enright, R. & Wang, E.N. Immersion Condensation on Oil-Infused Heterogeneous Surfaces for Enhanced Heat Transfer. *Sci. Rep.* **3**, 1988; DOI:10.1038/srep01988 (2013).



This work is licensed under a Creative Commons Attribution-NonCommercial-NoDerivs Works 3.0 Unported license. To view a copy of this license, visit <http://creativecommons.org/licenses/by-nc-nd/3.0>